Available online at www.sciencedirect.com
ScienceDirect
Journal of Solid State Chemistry 181 (2008) 855–862
JOURNAL OF SOLID STATE CHEMISTRY
www.elsevier.com/locate/jssc

Hydrothermal synthesis and luminescence of $CaMO_4:RE^{3+}$ (M = W, Mo; RE = Eu, Tb) submicro-phosphors

Fang Lei, Bing Yan*

Department of Chemistry, Tongji University, Siping Road 1239, Shanghai 200092, China

Received 30 October 2007; received in revised form 14 January 2008; accepted 20 January 2008
Available online 5 February 2008

Abstract

Submicrometer crystalline $CaMO_4:RE^{3+}$ (M = W, Mo; RE = Eu, Tb) phosphors with a sheelite structure have been synthesized via the hydrothermal process, which were characterized by X-ray powder diffraction (XRD), Fourier transform infrared spectroscopy (FT-IR), X-ray-excited luminescence (XEL), UV–vis diffuse reflectance spectra (UV–vis DRS) and scanning electron microscopy (SEM), respectively. The XRD patterns show that both $CaWO_4$ and $CaMoO_4$ have the same structure with space group $I41/a$. The SEM images indicate that the optimal hydrothermal temperature is 120 °C for the particles that aggregate with the increase of temperature. The bands ranging from 380 to 510 nm in the XEL spectra of $CaWO_4:Eu^{3+}$ can be attributed to the charge transfer state from the excited $2p$ orbits of O^{2-} to the empty orbits of the central W^{6+} of the tungstate groups. The comparison between photoluminescent lifetimes and quantum efficiencies of the two phosphors was also investigated in detail.

Keywords: Calcium tungstate; Calcium molybdate; Sheelite; Photoluminescence; X-ray-excited luminescence

1. Introduction

Metal tungstates and molybdates are two important families of inorganic materials that have great potential applications in various fields, such as phosphors, optical fibers, scintillators, magnets and catalysts [1–6]. There are two different structures for tungstate and molybdate compounds: wolframite and scheelite. The $CaMO_4$ (M = W, Mo) series belong to the scheelite structure and exhibit interesting X-ray luminescent properties. So they are used as X-ray phosphors, scintillators, laser crystal and host lattices in electron spin resonance [7–10]. Calcium tungstate has been extensively investigated as a self-activated phosphor emitting blue light related to tetrahedral WO_4 groups [11]. It is reported that $CaWO_4$ as an X-ray-intensifying screen material has been used for nearly 80 years. Among the scheelite-related phosphors, molybdate is a good choice as host material. Compared to tetrahedral WO_4 group, the central Mo^{6+} metal ion is coordinated to four oxygen atoms in the tetrahedral symmetry (T_d), and the cations, to eight oxygen atoms from different tetrahedral. Both molybdate and tungstate have broad and intense absorption bands due to charge transfer (CT) from oxygen to metal in the near-UV region. Many scheelite-related phosphors doped with Eu^{3+} have also been studied extensively and reveal a non-radiative mechanism for the energy transfer to the activator ion [10,12–17]. It is shown that $CaMO_4:Eu^{3+}$ (M = W, Mo) can be effectively excited by near-UV LEDs (380–410 nm), and then emits bright red fluorescence ($^5D_0$–$^7F_2$). Therefore, rare-earth ions-doped tungstates and molybdates are also potential materials for LED application.

In recent years, low-dimensional submicro-sized materials attracted much attention because of their unique small-size effect. To date, a variety of preparation techniques have been proposed to produce low-dimensional materials with controlled morphology [18,19], including microemulsion reaction [20], hydrothermal process, pulsed laser induced method [7], molten salt reaction [22], pechini method [23], sonochemical route [24], peptide-induced

*Corresponding author. Fax: +86 21 65982287.
E-mail addresses: Bingyan@tongji.edu.cn, byan@tongji.edu.cn (B. Yan).

0022-4596/$ - see front matter © 2008 Published by Elsevier Inc.
doi:10.1016/j.jssc.2008.01.033

precipitation method [25] and the sol–gel process. A great number of submicro-sized tungstate phosphors have been investigated for their potential application [21,22]. Hu and co-workers controllably synthesized $SrWO_4$ submicroparticles, submicropeanuts and submicrorods by a solvothermal-mediated microemulsion method [23]. Study on luminescent properties of submicro-sized phosphors is important due to their potential applications.

In this paper, we synthesized scheelite-type $CaMO_4$:Eu^{3+}/Tb^{3+} (M = W, Mo) phosphors via the hydrothermal process with a diameter of 30 nm of $CaWO_4$ and 40 nm of $CaMoO_4$. The morphology and size of $CaWO_4$ can be readily tuned by adjusting the experimental parameters. Because they are proper phosphors excited by X-rays [26], we also studied the XEL performance of the as-synthesized $CaMO_4$:Eu^{3+}/Tb^{3+} (M = W, Mo).

2. Experiments

$Na_2MoO_4 \cdot 2H_2O$ (AR), $Na_2WO_4 \cdot 2H_2O$ (AR), Eu_2O_3 (99.99%) and $Ca(NO_3)_2 \cdot 4H_2O$ (AR) were used as the starting materials, and all of them were of analytical grade without any further purification. $CaMO_4$:Eu^{3+} submicrophosphors were synthesized as follows: stoichiometric Eu_2O_3 was dissolved in nitrite acid under heating with continuous magnetic stirring. After the Eu_2O_3 was completely dissolved, the extra nitrite acid was removed by evaporation. Then deionized water was added to obtain $Eu(NO_3)_3$ solution. Meanwhile, appropriate amounts of $Na_2WO_4 \cdot 2H_2O$ and $Ca(NO_3)_2 \cdot 4H_2O$ were dissolved in deionized water to form aqueous solution. Then the $Eu(NO_3)_3$ and $Ca(NO_3)_2$ solutions were mixed homogeneously under magnetic stirring while Na_2WO_4 solution was being added. The two solutions were mixed with strongly magnetic stirring at room temperature to produce precipitate. The pH value was adjusted to about 9 with ammonia solution. Then the precipitate was transferred into a Teflon-lined stainless-steel autoclave with a filling capacity of 70%, and heated to a given temperature (120, 170 and 220 °C) and held for 24–72 h. Then the autoclave was cooled to room temperature naturally. The precipitate was collected by centrifugation, and washed three times with distilled water. After being dried in air at 60 °C for 24 h, the white powder product was obtained. The other powders were synthesized by the same procedure with the corresponding starting materials.

2.1. Physical measurements

X-ray powder diffraction (XRD) analysis was carried out on a Bruker D8 Focus powder diffractometer with Cu $K\alpha$ radiation (40 KV/60 mA, graphite monochromator). The morphology and particle size of the as-prepared powders were characterized by scanning electron microscopy (SEM) (JEOL, Model JEM-1230). X-ray-excited luminescence (XEL) spectra were measured at room temperature on a home-made X-ray-excited spectrometer, FluorMain, where a FII-30 movable X-ray tube (Tungsten anticathode target, 80 kV/4 mA) was used as the X-ray source and operated at room temperature. Photoluminescence spectra were measured by an RF-5301PC fluorescence spectrophotometer with a Xe lamp at room temperature. Fourier transform infrared spectroscopy (FT-IR) data were collected on a Perkin-Elmer 2000 FT-IR spectrophotometer in the range of 400–7000 cm^{-1} using KBr pellets. UV–vis diffuse reflectance spectra (UV–vis DRS) of dry pressed disk samples were obtained on a Lambda-900 UV–vis spectrophotometer and $BaSO_4$ was used as a reference standard. Luminescent lifetimes for the phosphors were characterized through an Ediburg FLS 920 phosphorimeter using a 450 W xenon lamp as the excitation source (pulse width, 3 μs).

3. Results and discussion

3.1. Basic characterization

Fig. 1 shows the XRD patterns of the submicrophosphor $CaWO_4$:Eu^{3+} and $CaMoO_4$:Eu^{3+} synthesized by the hydrothermal method at 120 °C for 72 h. All samples agrees well with the reported data (JCPDS: 41-1431 and 29-0351) and no other impurities could be found. Both $CaWO_4$ and $CaMoO_4$ are sheelite structures with the same space group $I41/a$ [88]. The unit cell parameters are $a = b = 5.243$ nm, $c = 11.373$ nm for $CaWO_4$ and $a = b = 5.226$ nm, $c = 11.430$ nm for $CaMoO_4$. The broadened peaks of the XRD patterns of the samples indicate the crystallite size is small. The approximate particle size of the product is evaluated from the (112) peak according to the Debye–Scherrer equation:

$$D = 0.89\lambda/(\beta \times \cos\theta), \quad (1)$$

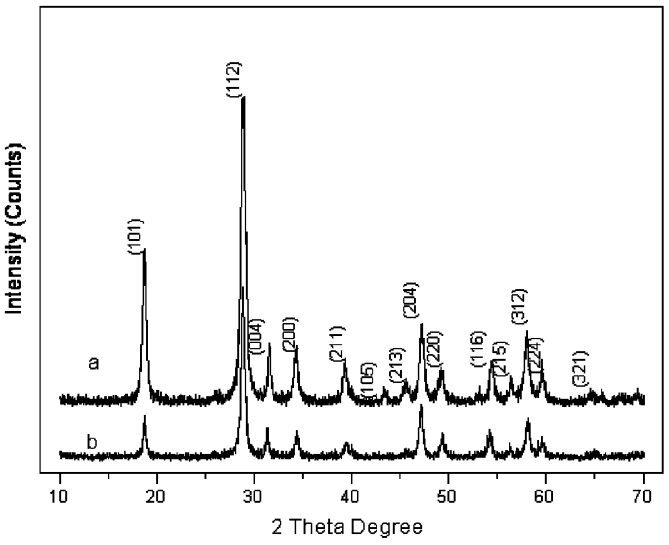

Fig. 1. XRD patterns of the samples of (a) $CaWO_4$:Eu^{3+} and (b) $CaMoO_4$:Eu^{3+} synthesized by the hydrothermal method at 120 °C.

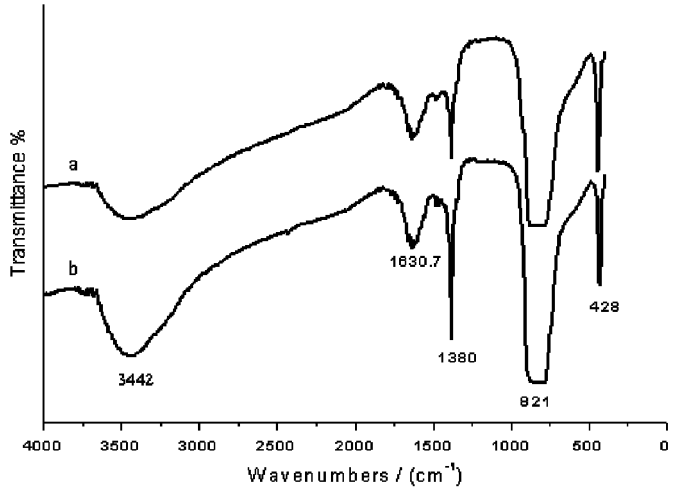

Fig. 2. FT-IR spectra of (a) $CaWO_4:Eu^{3+}$ and (b) $CaMoO_4:Eu^{3+}$.

Table 1
Vibrational wave numbers (cm^{-1}) and assignment for the $CaWO_4:Eu^{3+}$ and $CaMoO_4:Eu^{3+}$ synthesized by hydrothermal method at 120 °C [28]

Wave numbers (cm^{-1})	Assignment
3454	O–H
1630.7	O–H
1380	N–O
914–721	O–W–O
428	W–O

where D is the average grain size, λ represents Cu$K\alpha$ wavelength 0.1542 nm and β is the half-width of the peak with Bragg angle θ. The calculated results show that the average crystallite sizes of the $CaWO_4:Eu^{3+}$ and $CaMoO_4:Eu^{3+}$ powders are about 30 and 40 nm, respectively.

The FT-IR spectra of the as-synthesized samples $CaWO_4:Eu^{3+}$ and $CaMoO_4:Eu^{3+}$ phosphors by the hydrothermal method at 120 °C are shown in Fig. 2. The $CaWO_4:Eu^{3+}$ phosphor has approximate vibration modes as the $CaMoO_4:Eu^{3+}$ phosphor. Report on the FT-IR property of tungstate acids by Jesus et al. [27] shows that both have five vibrations modes, as described in Table 1. The bands at 3454 cm^{-1} and 1630.7 cm^{-1} are assigned to O–H stretching vibration and H–O–H bending vibration [4], respectively. The two bands are the characteristic vibrations of water from air, physically absorbed on the sample surface, which is completely different from coordinated water in compounds. The 1380 cm^{-1} band is attributed to N–O vibration modes probably from the remaining starting reactants NO_3^-. A strong absorption band around 910 cm^{-1} is related to O–W–O stretches of the WO_4 tetrahedron or to O–Mo–O stretches of the MoO_4 tetrahedron, because the AWO_4-type sheelite oxides, having S_4 site symmetry for the WO_4^{2-} groups, which show the main absorption bands in the region 400–1000 cm^{-1}, centered around 911, 833 and 405 cm^{-1} corresponding to the $\nu1$, $\nu3$ and $\nu2$ modes of the WO_4^{2-} groups, respectively [28]. For the same reason, the 428 cm^{-1} band is attributed to the $\nu2$ stretching vibration of W–O or Mo–O.

To understand the growth process of the submicrophosphors, we investigated the effects of temperature on the morphology of the products. Figs. 3(a–c) and 4(a–c) show the SEM images of the $CaWO_4:Eu^{3+}$ and $CaMoO_4:Eu^{3+}$, respectively, which synthesized at different temperatures (120, 170 and 220 °C) for 72 h. It clearly indicates that all products consist of nano- or micrometer spheres. When the reaction was carried out at 120 °C for 72 h, homogeneous spherical grains of $CaWO_4:Eu^{3+}$ with an average diameter of about 1 μm could be obtained (Fig. 3a). The diameter is bigger than the results calculated from the XRD pattern because the particles observed in SEM images are aggregated by many small crystal grains. While the reaction temperature was held at 170 °C, the grain size is not homogeneously dispersed. For the phosphor of $CaWO_4:Eu^{3+}$, when the temperature was increased to 220 °C, the particles tend to aggregate strongly and seem to melt into one phase. But the spherical grains still can be observed (Fig. 3c). Fig. 4(a–c) shows the morphology of $CaMoO_4:Eu^{3+}$ powders synthesized at 120, 170 and 220 °C. These images show that the small homogeneous grains aggregate to produce flake-like aspects. Compared with the SEM images of $CaWO_4:Eu^{3+}$, with increasing temperature, the morphology of $CaMoO_4:Eu^{3+}$ particles do not vary obviously. The mean size of $CaMoO_4:Eu^{3+}$ particles calculated by the Debye–Scherrer equation is about 40 nm.

3.2. Luminescent properties

The XEL spectra of $CaWO_4:Eu^{3+}$ and $CaMoO_4:Eu^{3+}$ powders are shown in Fig. 5. A broad luminescence band ranges from 375 to 510 nm in the spectrum of $CaWO_4:Eu^{3+}$, which agrees with the results of Yu [29]. It is attributed to the charge energy transfer of WO_4^{2-} in the $CaWO_4$ host. Nikl et al. [30] reported that the sheelite tungstate showed excitonic luminescence based on radiative transition within the tetrahedral (WO_4^{2-}) group, where the exciton becomes autolocalized. WO_4^{2-} has a tetragonal structure. W^{6+} is located in the center of the tetragonal structure with four O^{2-} located in the four apex angles. The outer shell of W^{6+} is full of electrons ($5s^25p^6$) in its ground state. When it is excited, one $2p$ electron of O^{2-} ($2s^22p^6$) transfers to W^{6+}'s $5d$ empty shells to form W^{5+} ($5s^25p^6d$), then transfers back to the ground state and generates transition radiation. The "spread-eagle" shape of the blue emission was explained by the influence of the Jahn–Teller effect on the degenerated excited state of (WO_4^{2-}) tetrahedron [31]; the peak at 615 nm is due to the $^5D_0$–$^7F_2$ electric dipole transition of the Eu^{3+} ion. $CaMoO_4$ has the same structure as $CaWO_4$. In the X-ray-excited luminescent spectrum, $CaMoO_4:Eu^{3+}$ phosphor has three main emission peaks at 592.8, 615 and 702.4 nm, which correspond to $^5D_0$–$^7F_1$, $^5D_0$–$^7F_2$ and $^5D_0$–$^7F_4$ transition of Eu^{3+} ion. The electric dipole

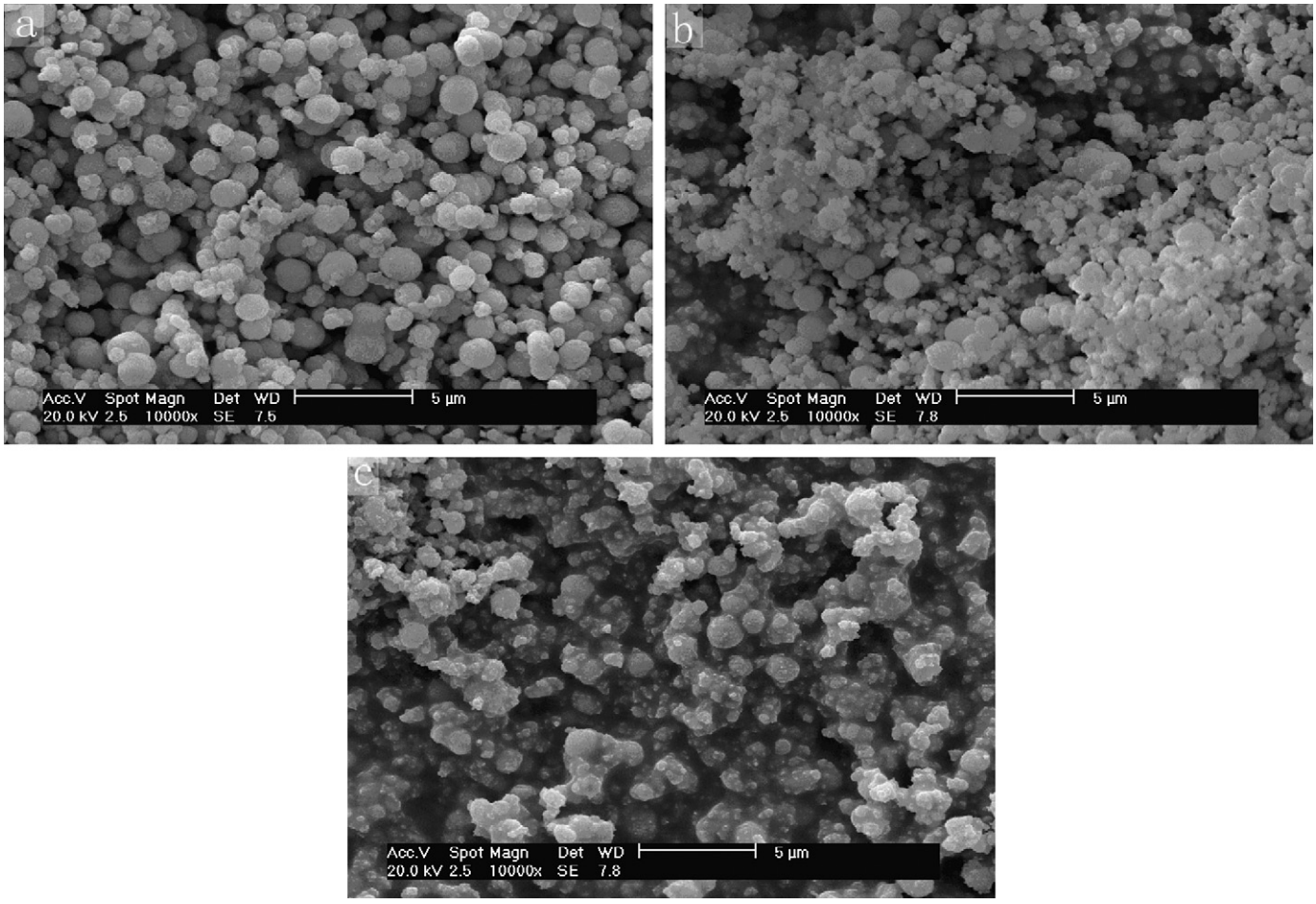

Fig. 3. SEM images of $CaWO_4:Eu^{3+}$ ((a) 120 °C, (b)170 °C and (c) 220 °C) phosphors synthesized by the hydrothermal method at different temperatures for 72 h.

transitions of $^5D_0$–$^7F_2$ is more prominent compared to the magnetic dipole transition of $^5D_0$–$^7F_1$ at 592.8 nm. Usually the intensity ratio of $^5D_0$–$^7F_2$ to $^5D_0$–$^7F_1$ is regarded as a probe to detect the inversion environmental symmetry around Eu^{3+} in the host [32]. If the RE^{3+} ions occupy the host sites with inversion symmetry, optical transitions inside the $4f^n$ configuration are strictly forbidden as electric dipole transition. So it can be concluded that the Eu^{3+} ion is not located at the site with inversion symmetry for both the phosphors. The XEL spectra show that $CaMoO_4$ is a more effective host material for rare-earth-doped phosphor than $CaWO_4$. The difference of the emission band ranging between 200 and 520 nm is due to the covalency discussed latter.

UV–vis absorption spectra of $CaWO_4:Eu^{3+}$ and $CaMoO_4:Eu^{3+}$ phosphors are shown in Fig. 6. According to the Li's research [33], $CaWO_4$ nano-crystals exhibited a very broad asymmetrical absorption in the range of 180–300 nm, which is also observed in Fig. 6. The absorption spectra of the two samples are very similar. The absorption band of $CaWO_4:Eu^{3+}$ is located between 210 and 300 nm, corresponding to oxygen to tungsten ($O \rightarrow W$) ligand-to-metal charge transfer (LMCT) in the WO_4^{2-} group [25]. At this absorption region, the peak of $CaMoO_4:Eu^{3+}$ is broader than $CaWO_4:Eu^{3+}$. The negative absorption peak at 614 nm is due to the $^5D_0$–$^7F_2$ transition of the Eu^{3+} ion excited by the UV component in the incident ray during the measurement.

Fig. 7 shows the comparison of the XEL spectrum of $CaWO_4:Tb^{3+}$ and $CaMoO_4:Tb^{3+}$ powders. $CaWO_4:Tb^{3+}$ phosphors emit bright green light under X-ray excitation, there are a group of typical $^5D_4$–^7F_J ($J = 6, 5, 4, 3$) transitions of Tb^{3+}. The predominant peak is attributed to the emission of $^5D_4$–$^7F_5$ at 545 nm. The other emissions located at 437, 489, 587 and 620 nm are ascribed to the transitions of $^5D_3$–$^7F_4$, $^5D_4$–$^7F_6$, $^5D_4$–$^7F_4$ and $^5D_4$–$^7F_3$, respectively. $CaMoO_4:Eu^{3+}$ also has the same peaks but with weaker intensities, because, except for the characteristic peak at 545 nm, other emission peaks of Tb^{3+} are obscure.

Fig. 8 shows the UV–vis DRS of (a) $CaWO_4:Tb^{3+}$ and (b) $CaMoO_4:Tb^{3+}$. Both have broad absorption band ranging from 200 to 480 nm and the spectrum of $CaWO_4:Tb^{3+}$ is steeper than that of $CaMoO_4:Tb^{3+}$, which is similar to Fig. 7. Both Figs. 6 and 8 indicate that MoO_4^{2-} has a broader absorption band than WO_4^{2-} in the UV-light region. Fig. 8 shows that the negative absorption peaks are the characteristic emission peaks of the active rare-earth ions, except for the emission band at 545 nm, on the UV–vis diffuse

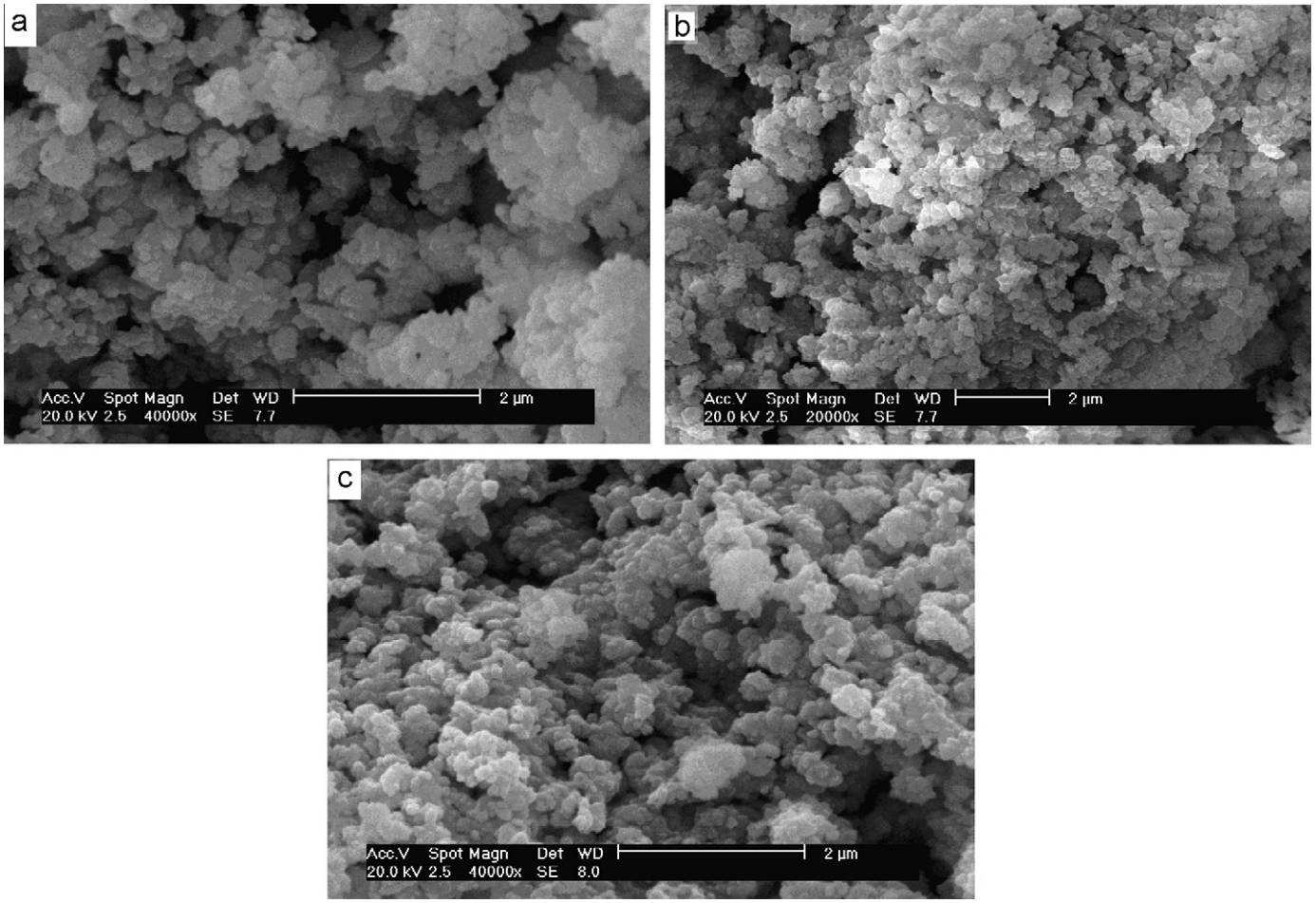

Fig. 4. SEM images of $CaMoO_4:Eu^{3+}$ ((a) 120 °C, (b) 170 °C and (c) 220 °C) phosphors synthesized by the hydrothermal method at different temperature for 72 h.

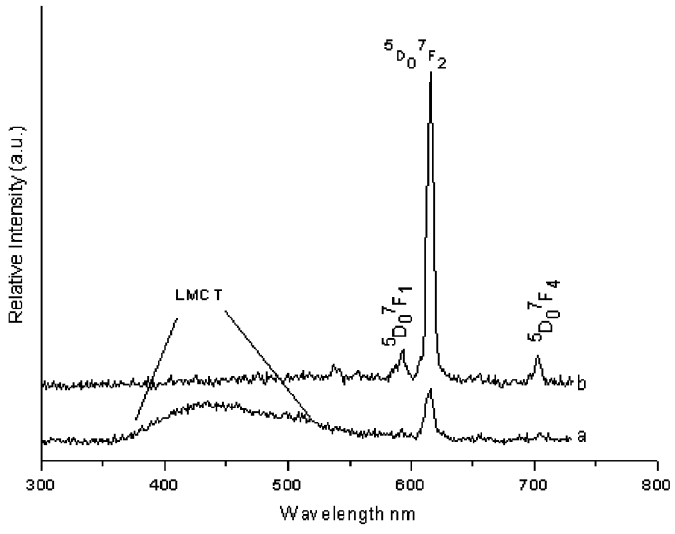

Fig. 5. The XEL spectra of (a) $CaWO_4:Eu^{3+}$ and (b) $CaMoO_4:Eu^{3+}$.

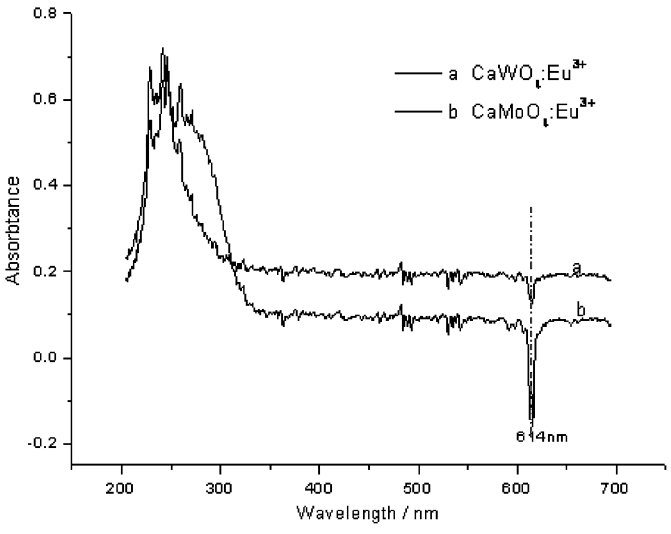

Fig. 6. UV–vis diffuse reflectance of (a) $CaWO_4:Eu^{3+}$ and (b) $CaMoO_4:Eu^{3+}$.

reflectance curve of $CaWO_4:Tb^{3+}$, there are three obvious characteristic emission peaks of Tb^{3+} at 490, 585 and 619 nm. While regarding $CaMoO_4:Tb^{3+}$, it has the 545 nm emission.

To further investigate the influence on the luminescent intensity of $CaWO_4:Eu^{3+}$ and $CaMoO_4:Eu^{3+}$ phosphors varied with the concentration of Eu^{3+}. The relationship

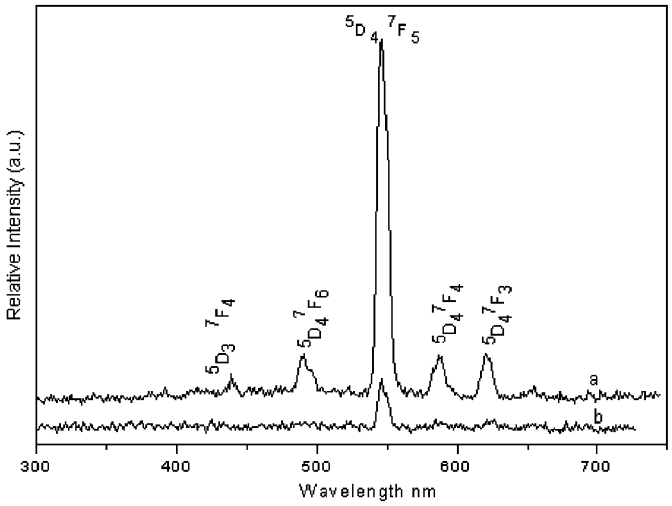

Fig. 7. XEL spectra of (a) $CaWO_4$:Tb^{3+} and (b) $CaMoO_4$:Tb^{3+}.

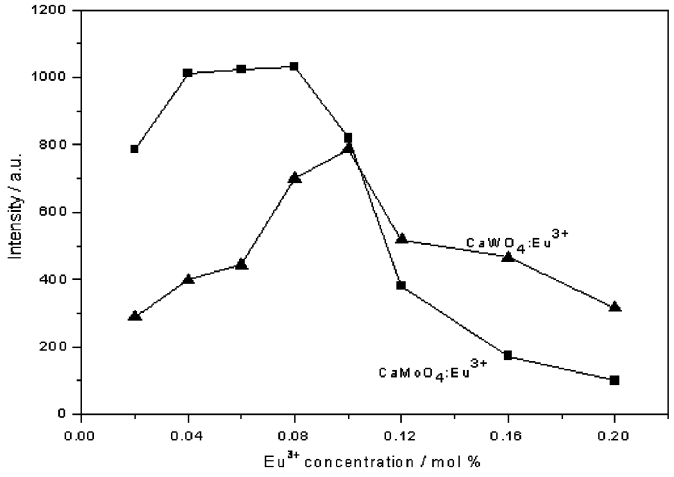

Fig. 9. Relationship between the 613 nm emission intensity of $CaWO_4$:Eu^{3+} and $CaMoO_4$:Eu^{3+} and concentration of doping Eu^{3+} concentration.

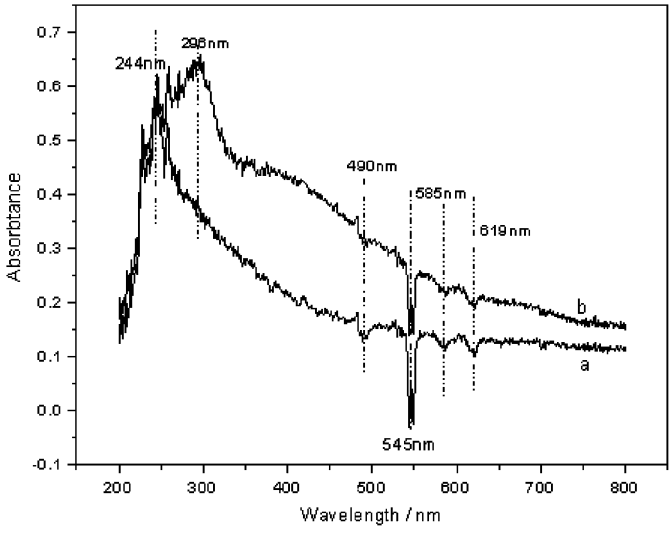

Fig. 8. UV–vis diffuse reflectance spectra of (a) $CaWO_4$:Tb^{3+} and (b) $CaMoO_4$:Tb^{3+}.

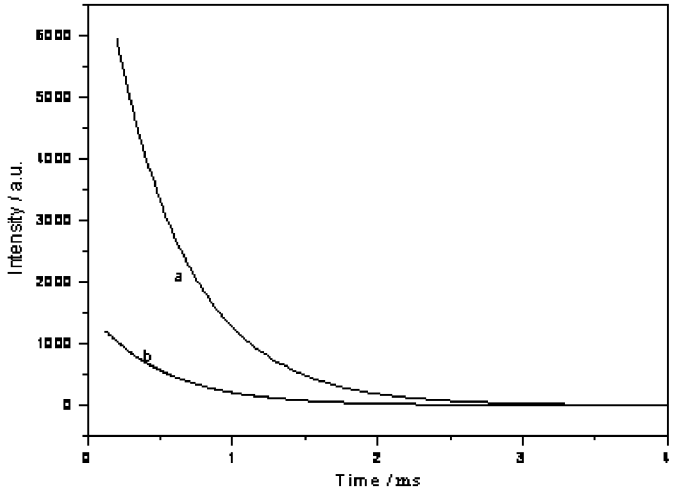

Fig. 10. Room temperature luminescence decay curves of the (a) $CaWO_4$:Eu^{3+} and (b) $CaMoO_4$:Eu^{3+} ($\lambda_{ex} = 393$ nm, $\lambda_{em} = 613$ nm).

between the emission intensity at 613 nm excited by 393 nm and concentration of Eu^{3+} is shown in Fig. 9. The luminescent intensity enhances with the increase of the doping concentration of Eu^{3+} and reaches a maximum at 10% for $CaWO_4$:xEu^{3+}, while for $CaMoO_4$:xEu^{3+}, 8% is the maximum doping concentration. When the Eu^{3+} concentration exceeds the quenching concentration, the intensity decreases and from the XRD pattern the second phase of Eu_2WO_6 can be observed.

The typical decay curve of $CaMO_4$:Eu^{3+} (M = W, Mo) was measured and described as a single exponential equation

$$\mathrm{Ln}(S(t)/S_0) = -k_1 t = -t/\tau,$$

which indicates that all Eu^{3+} ions occupy the same coordination environment. The fluorescence lifetime τ_1 of the $CaWO_4$:Eu^{3+} is about 516 μs and that of $CaMoO_4$:Eu^{3+} is about 494 μs. The luminescent decay curves (Fig. 10) of the $^5D_0$ excited state of Eu^{3+} are obtained by monitoring the $^5D_0 \rightarrow {}^7F_2$ emission. Further, the emission quantum efficiencies of the $^5D_0$ excited state of Eu^{3+} for $CaMoO_4$:Eu^{3+} and $CaWO_4$:Eu^{3+} were determined on the basis of the emission spectra and lifetimes of the $^5D_0$ emitting level, using the following four main equations according to Refs. [34–41]. The detailed principle and method were adopted as given in Ref. [42] and the data were shown in Table 1.

$$A_{0J} = A_{01}(I_{0J}/I_{01})(\upsilon_{01}/\upsilon_{0J}), \tag{2}$$

$$A_{\mathrm{rad}} = \sum A_{0J} = A_{01} + A_{02} + A_{03} + A_{04}, \tag{3}$$

$$\tau = A_{\mathrm{rad}}^{-1} + A_{n\mathrm{rad}}^{-1}, \tag{4}$$

$$\eta = A_{\mathrm{rad}}/(A_{\mathrm{rad}} + A_{n\mathrm{rad}}). \tag{5}$$

Here A_{0J} is the experimental coefficients of spontaneous emissions, A_{01} is the Einstein's coefficient of spontaneous emission between the $^5D_0$ and $^7F_1$ energy levels, which can be determined as approximately $50\,s^{-1}$ and as a reference to calculate the value of other A_{0J} [39–41]. I is the emission intensity and can be taken as the integrated intensity of the $^5D_0 \rightarrow {}^7F_J$ emission bands. υ_{0J} refers to the energy barrier and can be determined from the emission bands of Eu^{3+}'s $^5D_0 \rightarrow {}^7F_J$ emission transitions. A_{rad} and A_{nrad} are the radiative transition rate and non-radiative transition rate, respectively. A_{rad} can be determined from the summation of A_{0J} (Eq. (3)). Then the luminescence quantum efficiency can be calculated from the luminescent lifetimes, radiative and non-radiative transition rates. The luminescent quantum efficiency of $CaWO_4:Eu^{3+}$ (17.13%) is higher than that of $CaMoO_4:Eu^{3+}$ (12.78%) in spite of the slightly different lifetimes from each other, which is because the red/orange ratio of $CaWO_4:Eu^{3+}$ is more than that of $CaMoO_4:Eu^{3+}$.

Furthermore, to understand the effect of chemical environment on the luminescent property of Eu^{3+} better, we determined the Judd–Ofelt parameters for the Eu^{3+}-activated phosphors. The spontaneous emission probability, A, of the transition is related to its dipole strength according to [43–46]

$$A = (64e^2\pi^4\upsilon^3)/[3h(2J+1)] \times \{[(n^2+2)^2/9n]\sum \Omega_\lambda |<J||U^{(\lambda)}||J'>|^2, \quad (6)$$

where υ is the average transition energy in cm^{-1}, h is Planck's constant, and $2J+1$ is the degeneracy of the initial state (1 for $^5D_0$). The factors containing the medium's refractive index n result from local field corrections that convert the external electromagnetic field into an effective field at the location of the active center in the dielectric medium. The transition from $^5D_0$ to $^7F_1$ ($J=1$) is the isolated magnetic dipole transition and has no electric dipole contribution, which is practically independent of the chemical environment of the ion and can be used as a reference as mentioned above [42]. Besides, the $^5D_0 \rightarrow {}^7F_6$ transition could not be experimentally detected and it is not necessary to determine its J–O parameter. e is the electronic charge. With the refraction index $n = 1.506$ [44,45], and $|<J||U^{(\lambda)}|||J'>|^2$ values are the square reduced matrix elements whose values are 0.0032 and 0.0023 for $J=2$ and 4 [45,46], respectively. The Ω_2 and Ω_4 intensity parameters for the two phosphors are shown in Table 2. Ω_2 of $CaWO_4:Eu^{3+}$ (8.18) is higher than that of $CaMoO_4:Eu^{3+}$ (4.55), suggesting that the Eu^{3+} ion is located in a more polarizable chemical environment in $CaWO_4$ than in $CaMoO_4$. It means that $CaWO_4:Eu^{3+}$ possesses a stronger covalency than $CaMoO_4:Eu^{3+}$. The radius of Mo^{6+} is similar to that of W^{6+} for lanthanide contraction effect, while the interaction between W^{6+} and O is stronger than that of Mo^{6+}–O for the more electronic layer.

Table 2
Luminescence data for $CaMO_4:Eu^{3+}$ (M = W, Mo)

PL	$CaWO_4:Eu^{3+}$	$CaMoO_4:Eu^{3++}$
λ_{em} (nm)[a]	588.8, 613.7	576.2, 589.0, 613.4, 703.8
υ_{0J} (cm^{-1})	16983, 16295	17355, 16978, 16303, 14209
A_{0J} (s^{-1})	50, 282	26.4, 50, 170.5, 11.7
τ (ms)[b]	0.516	0.494
A_{exp} (s^{-1})	1938	2024
A_{rad} (s^{-1})	332	258.6
A_{nrad} (s^{-1})	1606	1766.4
η (%)	17.13	12.78
Ω_2 (10^{-20})	8.18	4.55
Ω_4 (10^{-20})	–	0.78
XEL	$CaWO_4:Eu^{3+}$	CaMoO4:Eu^{3++}
λ_{em} (nm)	569.6, 594.4, 614.9, 655.9, 702.9	592.36, 615.1, 702.1

[a]The relative intensities were obtained by the calculation of integrated area of the corrected emission bands.
[b]For $^5D_0 \rightarrow {}^7F_2$ transition of Eu^{3+}.

4. Conclusions

In conclusion, a series of submicro-crystal $CaMO_4:Eu^{3+}/Tb^{3+}$ (M = W, Mo) phosphors with 30–40 nm dimensions were prepared by the hydrothermal process. The morphology and dimension of $CaMO_4:Eu^{3+}$ (M = W, Mo) crystallites were influenced by hydrothermal temperature. The reaction temperature at 120 °C is the optimal hydrothermal temperature, for which we can obtain the homogeneous particles with a spherical shape of $CaWO_4:Eu^{3+}$. The emission bands from 380 to 510 nm in the XEL spectra of $CaWO_4:Eu^{3+}$ is attributed to the host lattice emission. The bands at about 615 nm are assigned to the characteristic $^5D_0$–$^7F_2$ emission of Eu^{3+} for both $CaMoO_4:Eu^{3+}$ and $CaWO_4:Eu^{3+}$. The luminescent intensity of the samples $CaWO_4:Eu^{3+}{}_x$ excited by 393 nm approaches a maximum at $x = 10\%$, while in $CaMoO_4:Eu^{3+}{}_x$, $x = 8\%$. The luminescent quantum efficiency of $CaWO_4:Eu^{3+}$ (17.13%) is higher than that of $CaMoO_4:Eu^{3+}$ (12.78%), different from the approximate of lifetime. We ascribe this to the different red/orange fluorescent band ratio of $CaWO_4:Eu^{3+}$ and $CaMoO_4:Eu^{3+}$.

Acknowledgments

This work was supported by the Developing Science Fund of Tongji University and the National Natural Science Foundation of China (20671072).

References

[1] H. Wang, F.D. Medina, Y.D. Zhou, Q.N. Zhang, Phys. Rev. B 45 (1992) 10356–10362.
[2] J. Geng, J.R. Zhang, J.M. Hong, J.J. Zhu, Int. J. Mod. Phys. B 19 (2005) 2734–2739.
[3] M. Moszyński, M. Balcerzyk, W. Czarnacki, A. Nassalski, T. Szczęśniak, H. Kraus, V.B. Mikhailik, I.M. Solskii, Nucl. Instrum. Methods Phys. Res. A 553 (2005) 578–591.

[4] A. Kato, S. Oishi, T. Shishido, M. Yamazaki, S. Iida, J. Phys. Chem. Solids 66 (2005) 2079–2081.
[5] M.V. Nazarov, B.S. Tsukerblat, E.J. Popovici, D.Y. Jeon, Phys. Lett. A 330 (2004) 291–298.
[6] G.X. Zhang, R.P. Jia, Q.S. Wu, Mater. Sci. Eng. B 128 (2006) 254–259.
[7] J.H. Ryu, S.Y. Bang, J.W. Yoon, C.S. Lim, K.B. Shim, Appl. Surf. Sci. 253 (2007) 8408–8414.
[8] Q.L. Dai, H.W. Song, X. Bai, G.H. Pan, S.Z. Lu, T. Wang, X.G. Ren, H.F. Zhao, J. Phys. Chem. C. 111 (2007) 7586–7592.
[9] J.S. Thorp, E.A.E. Ammar, J. Mater. Sci. 11 (1976) 1215–1219.
[10] M.V. Nazarov, D.Y. Jeon, J.H. Kang, E.J. Popovici, L.E. Muresan, M.V. Zamoryanskaya, B.S. Tsukerblat, Solid State Commun. 131 (2004) 307–311.
[11] J.P. Huang, H.S. Luo, P.L. Zhou, X.B. Yu, Y.K. Li, J. Lumin. 126 (2007) 881–885.
[12] L.G. Van Uitert, R.R. Soden, R.C. Linares, J. Chem. Phys. 36 (1962) 1793–1796.
[13] C.C. Torardi, C. Page, L. H Brixner, G. Blass, G.J. Dirksen, J. Solid State Chem. 69 (1987) 171–178.
[14] T. Kim, S. Kang, J. Lumin. 122–123 (2007) 964–966.
[15] S. Neeraj, N. Kijima, A.K. Cheetham, Chem. Phys. Lett. 387 (2004) 2–6.
[16] Z.L. Wang, H.B. Liang, J. Wang, M.L. Gong, Q. Su, Appl. Phys. Lett. 89 (2006) 0719211–0719213.
[17] L.N. Sun, M.H. Cao, Y.H. Wang, G.B. Sun, C.W. Hu, J. Cryst. Growth 289 (2006) 231–235.
[18] S.J. Chen, J. Li, X.T. Chen, J.M. Hong, Z.L. Xue, X.Z. You, J. Cryst. Growth 253 (2003) 361–365.
[19] J.K. Liu, Q.S. Wu, Y.P. Ding, J. Cryst. Growth 279 (2005) 410–414.
[20] M.L. Zorina, L.F. Syritso, J. Appl. Spectrosc. 16 (1972) 774–776.
[21] L.N. Sun, Q.R. Guo, X.L. Wu, S.J. Luo, W.L. Pan, K.L. Huang, J.F. Lu, L. Ren, M.H. Cao, C.W. Hu, J. Phys. Chem. C 111 (2007) 532–537.
[22] Y.G. Wang, J.F. Ma, J.T. Tao, X.Y. Zhu, J. Zhou, Z.Q. Zhao, L.J. Xie, H. Tian, Mater. Lett. 60 (2006) 291–293.
[23] C.A. Kodaira, H.F. Brit, M. Cláudia, F.C. Felinto, J. Solid State Chem. 171 (2003) 401–407.
[24] J. Geng, J.J. Zhu, H.Y. Chen, Cryst. Growth Des. 6 (2006) 321–326.
[25] G. Ahmad, M.B. Dickerson, B.C. Church, Y. Cai, S.E. Jones, R.R. Naik, J.S. King, C.J. Summers, N. Kröger, K.H. Sandhage, Adv. Mater. 18 (2006) 1759–1763.
[26] Y.L. Huang, Q. Feng, Y. Yang, H.J. Seo, Phys. Lett. A 336 (2005) 490–497.
[27] H.I.S. Nogueira, A.M.V. Cavaleiro, J. Rocha, T. Trindade, J.D. Pedrosa de Jesus, Mater. Res. Bull. 39 (2004) 683–693.
[28] S.P.S. Porto, J.F. Scott, Phys. Rev. 157 (1967) 716–719.
[29] Q. Zhang, W.T. Yao, X.Y. Chen, L.W. Zhu, Y.B. Fu, G.B. Zhang, L.S. Sheng, S.H. Yu, Cryst. Growth Des. 7 (2007) 1423–1431.
[30] M. Nikl, P. Bohacek, E. Mihokova, M. Kobayashi, M. Ishii, Y. Usuki, V. Babin, A. Stolovich, S. Zazubovich, M. Bacci, J. Lumin. 87–89 (2000) 1136–1139.
[31] K. Polak, M. Nikl, E. Mihokova, J. Lumin. 72–74 (1997) 781–785.
[32] F. Wang, X.P. Fan, D.B. Pi, Z.Y. Wang, M.Q. Wang, J. Solid State Chem. 178 (2005) 825–830.
[33] Y.G. Su, G.S. Li, Y.F. Xue, L.P. Li, J. Phys. Chem. C 111 (2007) 6684–6689.
[34] O.L. Malta, M.A.C. dosSantos, L.C. Thompson, N.K. Ito, J. Lumin. 69 (1996) 77–84.
[35] O.L. Malta, H.F. Brito, J.F.S. Menezes, F.R.G.E. Silva, S. Alves, F.S. Farias, A.V.M. deAndrade, J. Lumin. 75 (1997) 255–268.
[36] L.D. Carlos, Y. Messaddeq, H.F. Brito, R.A.S. Ferreira, V.D. Bermudez, S.J.L. Ribeiro, Adv. Mater. 12 (2000) 594–598.
[37] R.A.S. Ferreira, L.D. Carlos, R.R. Gonçalves, S.J.L. Ribeiro, V.D. Bermudez, Chem. Mater. 13 (2001) 2991–2998.
[38] P.C.R. Soares-Santos, H.I.S. Nogueira, V. Fe′lix, M.G.B. Drew, R.A.S. Ferreira, L.D. Carlos, T. Trindade, Chem. Mater. 15 (2003) 100–108.
[39] E.E.S. Teotonio, J.G.P. Espinola, H.F. Brito, O.L. Malta, S.F. Oliveria, D.L.A. de Faria, C.M.S. Izumi, Polyhedron 21 (2002) 1837–1844.
[40] S.J.L. Ribeiro, K. Dahmouche, C.A. Ribeiro, C.V. Santilli, S.H.J. Pulcinelli, J. Sol–Gel Sci. Technol. 13 (1998) 427–432.
[41] M.H.V. Werts, R.T.F. Jukes, J.W. Verhoeven, Phys. Chem. Chem. Phys. 4 (2002) 1542–1548.
[42] C.Y. Peng, H.J. Zhang, J.B. Yu, Q.G. Meng, L.S. Fu, H.R. Li, L.N. Sun, X.M. Guo, J. Phys. Chem. B 109 (2005) 15278–15287.
[43] G.F. de Sa, O.L. Malta, C.D. Donega, A.M. Simas, R.L. Longo, P.A. Santa-Cruz, E.F. da Silva, Coord. Chem. Rev. 196 (2000) 165–195.
[44] J.C. Boyer, F. Vetrone, J.A. Capobianco, A. Speghini, M. Bettinelli, J. Phys. Chem. B. 108 (2004) 20137–20143.
[45] C.A. Kodaira, A. Claudia, H.F. Brito, M.C.F. C Felinto, J. Solid State Chem. 171 (2003) 401–407.
[46] K. Binnemans, K. Van Herck, C. Goŕller-Walrand, Chem. Phys. Lett. 266 (1997) 297–302.